Title	Non-invasive sentinel lymph node mapping and needle guidance using clinical handheld photoacoustic imaging system in small animal
Author(s)	Sivasubramanian, Kathyayini; Periyasamy, Vijitha; Pramanik, Manojit
Citation	Sivasubramanian, K., Periyasamy, V., & Pramanik, M. (2018). Non-invasive sentinel lymph node mapping and needle guidance using clinical handheld photoacoustic imaging system in small animal. Journal of Biophotonics, 11(1), e201700061-.
Date	2017
URL	http://hdl.handle.net/10220/44326
Rights	

Article type: Original Paper

Non-invasive sentinel lymph node mapping and needle guidance using clinical handheld photoacoustic imaging system in small animal

Kathyayini Sivasubramanian, Vijitha Periyasamy, and Manojit Pramanik[*]

*Corresponding Author: E-mail: manojit@ntu.edu.sg, Phone: +65 67905835, Fax: +65 6791 1761

School of Chemical and Biomedical Engineering, Nanyang Technological University, 62 Nanyang drive, Singapore 637459

Keywords: (Photoacoustic imaging, sentinel lymph node mapping, handheld photoacoustic probe, clinical photoacoustic system, fine needle aspiration biopsy)

Translating photoacoustic imaging into clinical setup is a challenge. Handheld clinical real-time photoacoustic imaging systems are not common. In this work, we report an integrated photoacoustic and clinical ultrasound imaging system by combining light delivery with the ultrasound probe for sentinel lymph node imaging and needle guidance in small animal. The open access clinical ultrasound platform allows seamless integration of photoacoustic imaging resulting in the development of handheld real-time photoacoustic imaging probe. Both methylene blue and indocyanine green were used for mapping the sentinel lymph node using 675 nm and 690 nm wavelength illuminations, respectively. Additionally, needle guidance with combined ultrasound and photoacoustic imaging was demonstrated using this imaging system. Up to 1.5 cm imaging depth was observed with a 10 Hz laser at an imaging frame rate of 5 frames per second, which is sufficient for future translation into human sentinel lymph node imaging and needle guidance for fine needle aspiration biopsy.

1. Introduction

Invasive breast tumor is one of the leading causes of cancer deaths among women.[1] Diagnosing and staging it early is important for deciding treatment strategies, which plays an important role in the prognosis of the patient. In most cases of invasive breast tumors, surgical removal of primary breast tumor and axillary lymph node dissections (ALND) are common practice. There are lot of side effects associated with ALND including arm numbness, arm weakness, upper-extremity lymphedema, impaired shoulder mobility, and infections in breast, chest or arm.[2] Therefore, a more accurate, less complex and less invasive technique of sentinel lymph node biopsy (SLNB) was developed as an alternate. For node-negative breast cancer, SLNB has become the gold standard for initial screening.[3, 4] Lymph nodes are small oval-shaped organs that are present all through the body as part of the lymphatic system. They are connected via lymph vessels.[5] SLNB works on the assumption that sentinel lymph node will be the most probable primary site for metastases. Although this technique is more accurate and less complicated than ALND, its sensitivity is less than 95%.[6, 7] Also, there are side effects associated with SLNB procedure, including lymphedema, seroma formation, sensory nerve injury and limitation in the range of motion.[8] Therefore, it is very important to find non-invasive methods of identifying and staging the axilla without involvement of surgery (using fine needle aspiration biopsy) to overcome these limitations.

Ultrasonography (US) is an imaging technique that is commonly used to examine the axilla for pre-surgical assessment. US helps to visualise the size, shape, contour, texture, and other properties of lymph nodes which will differ if cancer cells have metastasised in comparison to normal lymph nodes.[9, 10] However, the accuracy of this technique is low, and it does not have the ability to identify and differentiate SLNs from other lymph nodes. Differentiating SLN is critical during the surgery to remove SLNs only and leave the other lymph nodes intact. The

possibility of false positive and false negative detections is also very high with this method. Therefore, US imaging cannot be used singularly for identifying, mapping, and staging of the breast cancer based on metastasis to SLNs.

Conventionally SLNB procedure involves injecting of methylene blue dye (or other dyes) and/or radioactive tracers to trace the lymphatic system and help in identifying the sentinel lymph node.[7, 11, 12] When both are used together the accuracy is improved.[13] The radioactive tracer has to be injected hours before the SLNB procedure, and methylene blue can be injected on the operating table itself as it moves quickly through the lymphatic system. After injection the region is cut open by making a small surgical incision. The surgeon then inspects the area visually to identify the blue coloured nodes in case of methylene blue to identify the SLN. To identify the SLN with radioactive tracer a Geiger counter is used. Few SLNs are then removed from the patient and subjected to histopathological studies to identify the presence or absence of cancer cells. Negative SLNB result indicates that cancer has not metastasised to nearby lymph nodes or other organs and a positive SLNB result indicates that cancer has metastasised to the sentinel lymph node and it is possible that it may be present in other nearby lymph nodes and, other organs. Although, this procedure is less invasive and complications associated are less severe than ALND, a non-invasive way of doing SLNB is very essential and highly beneficial for patients.

Dual modal photoacoustic imaging combined with ultrasound imaging for mapping SLN non-invasively has been demonstrated in several studies.[14-16] Photoacoustic imaging (PAI) is a hybrid dual modality imaging technique that enjoys the benefit of rich optical contrast and high ultrasonic resolution at depth.[17-20] In PAI, a short optical pulse is used for irradiating the tissue. The tissue absorbs the light due to which a small temperature rise occurs. Subsequently,

due to thermoelastic expansion pressure waves (or acoustic waves) are generated within the tissue. The acoustic waves [also called photoacoustic (PA) waves] are acquired using a wideband ultrasound transducer placed on the tissue surface. Images can be reconstructed from the PA signals to obtain the structural and functional information inside the tissue. The wide array of applications of PAI [14, 19, 21-23] stems from its advantages, namely deeper penetration depth, good spatial resolution and high soft tissue contrast. PAI contrast is dependent on optical absorption by molecules, which can be endogenous (blood, melanin, or even water) or exogenous (organic dyes, nanoparticles, quantum dots, etc.).[24-28]

A lot of work has been previously reported for SLN imaging and mapping in small animals as well as in humans using different contrast agents.[29-32] However, most of the reported photoacoustic systems cannot be used in clinics due to many factors. Few of which are: 1) immovable system design, hence is not convenient for clinical use, 2) use of non-clinical ultrasound transducers (as well as ultrasound machine) for data acquisition.[33, 34] Clinical translation with such transducers (system) is not possible; therefore use of clinical ultrasound imaging system is more preferred. Also, most of the reported work using clinical ultrasound systems is with systems that are not commercially available yet.[14, 15, 29] For PAI to be integrated with clinical ultrasound system, access to raw channel data is required, which was previously available in research based ultrasound systems only or custom made clinical ultrasound machine (not available to any researcher to purchase). Only recently, clinical ultrasound systems with access to raw channel data is made available commercially.[35] Another problem that has not been addressed sufficiently thus far is how SLNB surgery can be avoided by performing non-invasive needle guidance for fine needle aspiration biopsy. This will eliminate the complications associated with SLNB surgery. In this work, a clinical ultrasound system for combined US and PA imaging was used. For ease of use in clinical setup,

a custom made handheld holder for housing optical fiber and ultrasound transducer was fabricated. Two different dyes (methylene blue and indocyanine green) were used for identifying and mapping SLNs. Additionally, to eliminate the complications associated with the SLNB surgery, non-invasive real time needle tracking and guidance to remove the SLN tissue is also demonstrated.

2. Materials and Methods:

2.1. Photoacoustic and optical absorbance spectrum of the dyes used:

Methylene blue (MB) is a clinically approved and a widely used contrast agent for sentinel lymph node imaging.[15, 36] Indocyanine green (ICG) has also been explored for SLN imaging.[16] Therefore, these two dyes were used for all experiments in this work. From literature MB has an absorption peak around 668 nm,[37] and absorption of ICG is highly concentration dependent.[33] For experiments, 1000 µM concentration of ICG was chosen. The reported absorption peak for this concentration is 698 nm. In order to find an optimum wavelength to work, optical absorbance and PA spectrum of MB and ICG in the near infrared (NIR) wavelength range was recorded. To record the optical spectrum of the dyes, UV-visible spectrophotometer (Spectramax M5) was used. The wavelength was varied from 675 nm to 800 nm in steps of 5 nm. The concentration of MB and ICG used was 0.01 mg/mL and 0.00076 mg/mL, respectively. For animal blood photoacoustic spectrum, rat blood was used. For recording the PA spectrum, 10 mg/mL of MB (Sterop, Belgium) or ICG of 1000 µM concentration (I2633, Sigma Aldrich) or rat blood was injected into a transparent low density polyethylene (LDPE) tube of diameter 1.02 mm and placed in water bath. A single element ultrasound transducer (2.25 MHz center frequency, V306-SU, Olympus-NDT) was used for PA signal acquisition. The signals were first amplified, and then band pass filtered by ultrasound signal receiver (R/A/F) unit (5072PR, Olympus-NDT), and then digitized and stored in a

desktop with data acquisition (DAQ) card (compuscope 4227, GaGe). The OPO laser (Continuum, Surelite OPO) used here has a minimum wavelength of 670 nm. However, there is a lot of fluctuation in the starting wavelength. Therefore, laser was varied from 675 nm to 800 nm wavelength with a 5 nm step size similar to optical spectrum. Each of the obtained PA signals was averaged 10 times. The peak-to-peak PA signal intensity is plotted against the wavelength. The PA signals were normalized with the laser power.

2.2. Clinical handheld photoacoustic imaging system:

For excitation, light from an OPO (Continuum, Surelite OPO) laser pumped by a frequency doubled nanosecond pulsed Nd:YAG pump laser (Continuum, Surelite Ex) was used. The OPO generates 5 ns duration pulses and has a 10 Hz pulse repetition rate with tunable wavelengths from 670 nm to 2500 nm. A clinical research ultrasound system (E-CUBE 12R, Alpinion, South Korea), capable of dual modal imaging (PA and US imaging), was used for signal acquisition. To operate the system in PA mode, laser excitation needs to be provided. The trigger from the laser synchronized the laser excitation and E-CUBE data acquisition. The generated PA signals were acquired with a linear array transducer L3-12 with center frequency of ~8.5 MHz and 95% fractional bandwidth. The axial resolution of the system was calculated to be 207±45 µm up to an imaging depth of 3 cm. The axial resolution is very consistent with various imaging depths. The lateral resolution of the system is dependent on the ultrasound array element size, which is 300 micron for the probe we used. For imaging experiments the laser was tuned to 675 nm for MB (10 mg/mL) and 690 nm for ICG (1000 µM). The light from the laser was coupled to the sample with a bifurcated optical fiber bundle (Ceramoptec GmbH, Germany) with 1600 optical fibers. Each fiber has a core diameter of 185 µm (200 µm with cladding) with a numerical aperture of 0.22. The two output ends of the fiber bundle were fixed in the custom made (3D printed) probe holder along with the linear array ultrasound transducer to make a handheld

system. The angle of illumination of light for this holder was 15°. The different probe holder parameters were optimized for SLN imaging using Monte carlo simulations for light delivery and PA imaging with SLN mimicking phantoms.[38] The energy loss due to fiber coupling was approximately 40%. The light energy on the sample surface was ~25 mJ per pulse at 675 nm. The fluence on the surface of the sample calculated to be ~8.34 mJ/cm^2 (total area of illumination from both ends together is ~3 cm^2). Thus, the fluence was well within the American National Standards Institute (ANSI) safety limit of 20 mJ/cm^2.[39] The processed beam-formed PA images were displayed on the E-CUBE monitor at 5 frames per second (fps) frame rate, since two laser pulses are required to form one PA image.

2.3. Data acquisition and image formation:

The clinical E-CUBE ultrasound system has the capability to perform US and PA separately as well as dual-mode imaging (US and PA) simultaneously.[35] Here, it was operated in combined mode only. This could be done by operating the system in research mode. In this mode, different parameters can be specified using python code. Few of them are, imaging depth, number of frames to be saved, and the type of data (Radiofrequency data, beam-formed data, scan-converted data or I.Q. data) to be saved. The total imaging depth was set at 2 cm. The imaging data was stored as beam-formed datatype. Different transducers are compatible with this system. For this work, linear array (L3-12) transducer was used. The L3-12 transducer has 128 array elements with 8.5-MHz center frequency (95% fractional bandwidth). The active area of the transducer is 3.85 cm × 1cm. E-CUBE system has 64 parallel DAQ hardware. Thus, for each laser pulse fired; data is collected by 64 channels only. Therefore, two laser pulses are needed to obtain data from all 128 channels. Following two laser pulses, the system combines the PA signal obtained from two pulses into a single image. The final processed image is displayed on the E-CUBE monitor after it passes through a series of inbuilt filters. Since two laser pulses are

needed to collect a complete PA b-scan image, the frame rate of the imaging system is 5 frames per second (the OPO laser operates at 10 Hz). Higher repetition rate laser can increase the frame rate of the PA imaging, also reducing the imaging area by using only 64 channels for data acquisition will increase the imaging frame rate. Up to 7000 frames per second photoacoustic imaging was demonstrated with this system earlier.[40]

2.4. Animal preparation:

Animal experiments were performed in accordance with the approved guidelines and regulations, and were approved by the Institutional Animal Care and Use committee of Nanyang Technological University, Singapore (Animal Protocol Number ARF-SBS/NIE-A0263). For experiments, 6 healthy adult female Sprague dawley rats of weight 225 ± 25 gm (aged 8 - 10 weeks) were procured from InVivos Pte. Ltd., Singapore. Two animals (both sides of the rat was imaged) each for imaging with saline, MB and ICG were used. Firstly, before performing *in vivo* imaging the rats were anesthetized. Anaesthesia mixture contains Ketamine and Xylazine (dosage of 85 mg/kg and 15 mg/kg, respectively). An intraperitoneal injection of 0.2 ml per 100 g of the rat body weight was given. Subsequently, the animal was prepared for imaging by removing hair in the region of interest using commercially available hair removal cream. A custom made nose cone covered with a breathing mask covering the mouth and nose of the animal was used to deliver the anaesthesia mixture. During experiments, animal was maintained under anaesthesia all through with the help of isoflurane gas (Medical Plus Pte Ltd, Singapore). 0.75% of isoflurane was administered along with oxygen (1.2 L/min). A pulse oximeter (Medtronic, PM10N with veterinary sensor) was used to monitor the heart rate and peripheral oxygen saturation during experiments. The animal was placed sideways and combined PA and US images were recorded with the handheld probe before and after dye

injection. After acquisition of the PA images, the animals were euthanized with a pentobarbital overdose. Finally the SLNs were dissected out for study.

2.5. Sentinel lymph node imaging in rats:

The schematic representation of the imaging system is shown in **Figure 1**. To image SLN a custom made handheld probe holder housing the ultrasound transducer and optical fiber for light delivery was used. The probe holder design was optimised for SLN imaging in our previous work.[38] The parameters used for imaging are fiber to probe distance of approximately 2 cm, fiber to tissue distance of 1 cm, and angle of light illumination of 15°. In rats SLN is usually present just below the skin surface. To emulate a more realistic human SLN imaging scenario a 0.5 cm chicken breast tissue (CBT) was placed on top of the rat. Ultrasound gel was spread on top of the tissue for better ultrasound coupling. Using the handheld PA imaging system the sentinel lymph nodes in rats were imaged before and after the injection of the dye (saline or MB or ICG). Saline was used as a control study. Control image of the SLN was taken before the dye injection. 0.2 mL of the dye (MB or ICG) was injected in the forepaw of the imaging side of the animal. The forepaw of the animal was massaged for 5 min to promote the movement of the dye in to the lymph nodes. Following which the lymph nodes were imaged and identified using the handheld PA probe. For confirmatory studies wavelength was varied from 670 nm to 800 nm at a speed of 10 nm/s while holding the probe at a fixed location. The spectroscopic data from the SLN was later compared to the spectroscopic data obtained *in vitro*. Also, to cover all realistic scenarios for human SLN imaging, up to 1.5 cm deep imaging was done with the help of additional chicken tissue slices.

2.6. Needle tracking:

Non-invasive imaging and mapping of sentinel lymph nodes is the preliminary step in staging of breast cancer. The imaging region needs to be cut open to remove the lymph nodes for biopsy, which is a painful procedure and has lot of complications associated with it. We have shown here real time needle guidance (minimally invasive) to remove tissue from SLN for further biopsy. This is done at 675 nm and 690 nm where there is maximum optical absorption for MB and ICG, respectively. After identification of sentinel lymph nodes in rats, the combined handheld PA probe holder was held steady in that position. A 23G needle (BD PrecisionGlide Needle) of dimensions 0.6 mm × 32 mm was slowly inserted into the animal through the chicken tissue parallel to the longer side of the ultrasound transducer while tracking it in real time on the E-CUBE's monitor. When the needle reaches the sentinel lymph node some tissue can be extracted out on which further histopathological studies can be done for staging the tumor, if any is present.

3. Results and Discussion

MB is a Food and Drug Administration (FDA) approved dye and is widely used clinically for SLNB. Therefore, MB (due to its strong light absorption) has been used for noninvasively imaging sentinel lymph node with photoacoustic imaging extensively.[14, 15, 36] ICG is another dye that is being explored for SLN imaging.[16, 33] Both these dyes are used as PA contrast agents in this study. In order to determine the most suitable wavelength in the NIR region for both the dyes, UV-visible and PA spectrum was recorded *in vitro*. To compare with the feasible experimental conditions, UV-visible spectrum is recorded in the wavelength range of 675 to 800 nm. The UV-visible spectrum of methylene blue and ICG is shown in **Figure 2(a) and 2(c)**, respectively. The PA spectrum of MB and ICG is shown in **Figure 2(b) and 2(d)**, respectively. It is to be noted that the maximum peak-to-peak PA signal intensity is at 675 nm and 690 nm for MB and ICG, respectively and hence, chosen for experiments. It can be

observed that the PA spectrum of MB and ICG is in correlation with their respective optical absorption. The PA spectrum of rat blood is shown in **Figure 2 (e).** All the spectrum shown in Figure 2 are normalized individually.

After determining the optimum wavelength for imaging, animal experiments were performed. Saline was used as control as it does not have light absorption in the NIR range and does not produce any contrast for photoacoustic imaging. **Figure 3(a)** shows the photograph of the shaved regions of a rat for SLN imaging. Black dotted line shows roughly the plane across which B-scan ultrasound as well as photoacoustic imaging were done. All combined PA and US images shown are screenshots taken from the E-CUBE monitor. **Figures 3(b) and 3(c)** show the combined US and PA images before and after injection of saline. It is to be noted that we can identify the lymph nodes with the help of ultrasound only, but the contrast is not very high and it needs a trained eye to identify them. Even though ultrasound imaging can identify the lymph node, it cannot differentiate the sentinel one. As expected, there is no PA signal before and after injection of saline, thus, saline cannot help mapping the SLN with PA imaging. **Figure 3(d)** shows the photograph of the sentinel lymph node after skin removal once imaging was finished. **Figure 3(e)** shows the photograph of the excised SLN from the rat. It can be noted from the image that SLN is not coloured, but it is bulged indicating that it is completely perfused with saline. **Figure 3(f) and 3(g)** show the combined US and PA images before and after injection of MB, respectively. The gray colors represent the US image and the coloured part shows the PA images. It can be observed that there is no PA signal before injection of MB in the SLN area. But after injection of MB, there is an increased PA signal in the SLN, and therefore, it is visible in Figure 3(g). **Figure 3(h)** shows the photograph of the SLN with MB after skin removal. The blue coloured stains helps in easy identification with naked eyes. The image also shows the lymph vessels filled with the MB. **Figure 3(i)** shows the photograph of the excised SLN completely filled with MB. From this image we can compare and confirm the

size of the SLN with the combined US and PA image. Similarly**,** **Figures 3(j) and 3(k)** show the combined US and PA images before and after injection of ICG. It is evident from the images that there is no PA signal from the SLN before injection of ICG, but after injection the PA signal is very prominent. **Figure 3(l)** shows the photograph of the SLN with ICG after removing the skin. The SLN is not obviously stained visually as opposed to MB (since ICG solution is colorless or light greenish in appearance). Nevertheless, they are perfused with ICG solution which helps in differentiating them from other normal lymph nodes. **Figure 3(m)** shows the photograph of the excised SLN completely filled with ICG. As stated earlier, from the image we can compare and confirm the size and location of SLN with the combined US and PA image.

The optical absorption of MB is wavelength dependent, whereas for ICG it is concentration dependent as well. MB has a peak around 670 nm and the peak is quite sharp. In comparison ICG has broader absorption profile in the NIR region. It is expected that the wavelength dependent absorption will reflect in the *in vivo* SLN imaging. For confirmatory studies spectral analysis was used by varying the wavelength from 670 nm and 800 nm and imaged in real time on the E-CUBE's monitor. This helped in providing evidence that the PA signal was from SLN filled with the dye only. The combined PA and ultrasound imaging as the laser wavelength was scanned is shown movie S1 and movie S2 (for MB and ICG, respectively). In case of MB, as the absorption peak is sharp, the PA signal disappears quickly in the movie as the laser wavelength is scanned. Confirming the PA signal is from the SLN filled with MB. Similarly, in case of ICG, the PA signal decreases rather slowly, but does not disappear completely unlike the case of MB, as the absorption peak of ICG is much wider in the chosen wavelength range. Also, while varying the wavelength from 670 nm to 800 nm, the PA signals were recorded and saved as beam formed data. From the saved data, the signal-to-noise ratio (SNR) from the SLN area is calculated at different wavelengths and plotted as PA spectrum of *in vivo* data.

Additionally, for comparison PA spectrum (in terms of SNR) is obtained from the nearby blood vessel at various wavelengths. All the spectrums are compensated for the laser power variation at different wavelengths, and then they were individually normalized by the maximum SNR. **Figures 4(a) and 4(b)** show the PA spectrum from SLN for MB and ICG, respectively. **Figure 4(c)** shows the PA spectrum obtained from the blood vessel from a nearby region. It can be noted that the trend in the PA spectrum from the SLN in rat matches with the PA spectrum obtained with the respective dyes *in vitro* [Figure 2(b) and 2(d)]. While the PA spectrum of MB and ICG is decreasing, it can be noted that there is not much change in the PA spectrum of blood vessel, which matches well with the *in vitro* PA spectrum of blood [Figure 2(e)].

In human, SLNs are usually located within 1-2 cm depth below the skin surface. In rats, the SLN is located right beneath the skin (few mm depth). Therefore, to mimmic SLN imaging in humans, chicken breast tissue was placed on the top of the skin surface of the rats, thus the SLN lies 0.5-1.5 cm below the chicken tissue surface. The thickness of the chicken breast tissue was increased in steps of 0.5 cm on top of the rat skin. The thickness of the chicken breast tissue was increased in steps of 0.5 cm on top of the rat to simulate depth imaging. Imaging was done at 675 nm and 690 nm for MB and ICG, respectively. The combined US and PA images of SLN filled with MB at different depths of 0.5 cm, 1 cm, and 1.5 cm is shown in **Figure 5 (a), 5(b) and 5(c),** respectively. Similarly, combined US and PA images of SLN with ICG at various depths of 0.5 cm, 1 cm, and 1.5 cm is shown in **Figure 5 (d), 5(e) and 5(f),** respectively. It can be noticed from the images that the SLN is clearly visible even at higher depths for both the dyes. Additionally, SNR was also calculated from the SLN at different depths. SNR was defined as the amplitude of the PA signal from the SLN divided by the standard deviation of the background noise, $SNR = \frac{V}{n}$, here V is the PA signal amplitude from SLN, and n is the standard deviation of the background noise. The calculated SNR for MB at depths of 0.5 cm, 1 cm, and

1.5 cm are 33.40, 57.9, and 21.02, respectively. The SNR for ICG was calculated to be 11.17, 5.6, and 2.15 for depths of 0.5 cm, 1 cm, and 1.5 cm, respectively. SNR at 1 cm is highest in case of MB which is consistent with our simulation and phantom results published earlier, due to the light delivery angle.[38] With ICG the SNR decreases with increase in depth, which is as expected. From the figures, it can be concluded that both ICG and MB are viable and effective contrast agents for SLN imaging in a clinical scenario.

Non-invasive identification together with fine needle aspiration biopsy (FNAB) of SLN will reduce complications associated with SLNB surgery. Ultrasonography is the most commonly used technique for needle guidance, catheter placement, etc. till now.[41] But, the contrast provided by ultrasound is not great to visualize needle going inside tissue. Non-invasive, real time needle guidance for biopsy of SLN with photoacoustic imaging is also shown here. As soon as SLN was identified in the rat by PA imaging, the probe holder was held fixed in the position. A 23G needle was inserted parallel to the longer side of the ultrasound transducer and guided to the SLN by real-time monitoring of the needle on the E-CUBE's screen. **Figure 6 (a)** shows the image of US guided needle biopsy by the needle into the SLN. **Figure 6 (b) and 6(c)** show the combined US and PA images of the guided needle biopsy of the SLN. For comparison pure US guided imaging was also performed. The contrast provided by US was quite poor and one needs a trained eye to follow the needle and guide it properly [Figure 6(a)]. On the other hand, with PA imaging, the contrast from the needle is very high and can be easily monitored *in vivo* [Figure 6(b) and 6(c)]. Once, the needle reaches the SLN a small portion of the SLN tissue can be taken out for histological examination. The movie showing the real time needle guidance under plain ultrasound is shown in movie S3. The movies of real time needle guidance with combined US and PA imaging with MB and ICG injection to the SLN is shown in movie S4, and movie S5, respectively. It is to be noted that the artifact above the needle is due to the

reconstruction and post-processing algorithm used by the ultrasound system. The needle can be differentiated from the artifact based on the higher signal intensity in comparison to the artifact. Additionally, the signal from the needle is a single straight line across depth while the signal from the artifact is divergent with depth. These factors will help in identifying and differentiating the needle from the artifact. The artifact is not present when homemade reconstruction algorithm was used with the raw RF channel data to form the PA images. However, such homemade reconstructed PA images cannot be feed back to the ultrasound machine for real-time display at the moment.

The cost associated with screening, diagnosis and treatment of breast cancer is very high, and the number of cases reported is increasing every year. Therefore, a cost effective, fast, less complicated, and more efficient imaging and guidance system is much needed. Combined US and PA imaging is one such technique which can be used for effective screening, diagnosis and staging of breast cancer. There is lot of research going on to explore the potential of this technique. This is easily feasible with FDA approved contrast agents such as MB, which is already being used routinely for SLNB procedure. The number of false positives and false negatives can also be decreased significantly using dual modality imaging. Since, it is a non-invasive procedure the complications and pain associated with surgery will be eliminated for patients. In this work, we have demonstrated using a dual modal photoacoustic and ultrasound system (based on a clinical ultrasound platform) SLN can be identified using both MB as well as ICG. Moreover, under PA imaging the needle guidance in real time for FNAB in place of SLNB surgery can also be improved. There are few challenges associated with this technique. Firstly, the lasers currently used for PA imaging are very bulky, and portable high energy pulsed lasers although available, are quite expensive. Secondly, the integration of light delivery with the ultrasound probe is also a challenging task with high laser light coupling efficiency. Lastly,

MB has an absorption peak ~665 nm wavelength. Currently, availability of lasers at this wavelength is limited. Therefore, most researchers are using 670-675 nm lasers. Although the difference in wavelength is very small, but there is a significant difference in light absorption (since MB absorption peak is very sharp).

4. Conclusion

In this work, we have demonstrated that a commercial clinical ultrasound system can be used for combined US and PA imaging of SLN in small animals (rat). To provide imaging contrast, MB and ICG were used as they have high optical absorption in the NIR wavelength region. Moreover, MB is already been used in clinic for SLNB, therefore, it will not affect the clinical workflow. Spectral studies were done to confirm that the SLN images obtained are due to the lymph node filled with the dye. SLN imaging at varying depths of up to 1.5 cm was done to make it suitable for clinical scenario. Additionally, non-invasive needle guidance for FNAB was performed by tracking the needle in real time under photoacoustic imaging. This will be very useful in eliminating the necessity for SLNB surgery and thereby avoiding the complications associated with it.

Supporting Information

Additional supporting information may be found in the online version of this article at the publisher's website.

Movie S1: Movie showing the combined US and PA imaging of SLN with MB *in vivo* while varying the wavelength from 670 to 800 nm.

Movie S2: Movie showing the combined US and PA imaging of SLN with ICG *in vivo* while varying the wavelength from 670 to 800 nm.

Movie S3: Movie showing non-invasive, real time needle guidance for FNAB of SLN with US imaging only.

Movie S4: Movie showing non-invasive, real time needle guidance for FNAB of SLN with MB with combined US and PA imaging.

Movie S5: Movie showing non-invasive, real time needle guidance for FNAB of SLN with ICG with combined US and PA imaging.

Acknowledgements

The authors would like to acknowledge the financial support from the Tier 1 research grant funded by the Ministry of Education in Singapore (RG48/16: M4011617) and Tier 2 research grant funded by Ministry of Education in Singapore (ARC2/15: M4020238). Authors have no relevant financial interests in the manuscript and no other potential conflicts of interest to disclose.

Author biographies

Please see Supporting Information online.

References

[1] in International Agency for Research on Cancer, Vol. (Ed.^Eds.: Editor), City, **2013**.

[2] K. K. Swenson, M. J. Nissen, C. Ceonsky, L. Swenson, M. W. Lee, T. M. Tuttle *Ann. Surg. Oncol.* **2002**, *9*, 745-753.

[3] K. M. McMasters, T. M. Tuttle, D. J. Carlson, C. M. Brown, R. D. Noyes, R. L. Glaser, D. J. Vennekotter, P. S. Turk, P. S. Tate, A. Sardi, P. B. Cerrito, M. J. Edwards *J. Clin. Oncol.* **2000**, *18*, 2560-2566.

[4] D. Krag, D. Weaver, T. Ashikaga, F. Moffat, V. S. Klimberg, C. Shriver, S. Feldman, R. Kusminsky, M. Gadd, J. Kuhn, S. Harlow, P. Beitsch *N. Engl. J. Med.* **1998**, *339*, 941-946.

[5] L. G. Albertini JJ , Cox C , et al . *The Journal of the American Medical Association*. **1996**, *276*, 1818-1822.

[6] O. A. Ung, N. South, W. Breast, W. Hospital *Asian J. Surg.* **2004**, *27*, 284-290.

[7] D. Krag, D. Weaver, T. Ashikaga, F. Moffat, V. S. Klimberg, C. Shriver, S. Feldman, R. Kusminsky, M. Gadd, J. Kuhn, S. Harlow, P. Beitsch *N. Engl. J. Med.* **1998**, *339*, 941-946.

[8] A. D. Purushotham, S. Upponi, M. B. Klevesath, L. Bobrow, K. Millar, J. P. Myles, S. W. Duffy *J. Clin. Oncol.* **2005**, *23*, 4312-4321.

[9] B. Brancato, M. Zappa, D. Bricolo, S. Catarzi, G. Risso, R. Bonardi, P. Cariaggi, A. Bianchin, P. Bricolo, M. Rosselli Del Turco, L. Cataliotti, S. Bianchi, S. Ciatto *Radiol. Med.* **2004**, *108*, 345-355.

[10] S. Krishnamurthy, N. Sneige, D. G. Bedi, B. S. Edieken, B. D. Fornage, H. M. Kuerer, S. E. Singletary, K. K. Hunt *Cancer*. **2002**, *95*, 982-988.

[11] S. K. Somasundaram, D. W. Chicken, M. R. S. Keshtgar *Br. Med. Bull.* **2007**, *84*, 117-131.

[12] P. J. Borgstein, S. Meijer, R. Pijpers *The Lancet*. **1997**, *349*, 1668-1669.

[13] Z. Radovanovic, A. Golubovic, A. Plzak, B. Stojiljkovic, D. Radovanovic *Eur. J. Surg. Oncol.* **2004**, *30*, 913-917.

[14] A. Garcia-Uribe, T. N. Erpelding, A. Krumholz, H. Ke, K. Maslov, C. Appleton, J. A. Margenthaler, L. V. Wang *Sci. Rep.* **2015**, *5*, 15748.

[15] T. N. Erpelding, C. Kim, M. Pramanik, L. Jankovic, K. Maslov, Z. Guo, J. A. Margenthaler, M. D. Pashley, L. V. Wang *Radiology*. **2010**, *256*, 102-110.

[16] C. Kim, T. N. Erpelding, K. Maslov, L. Jankovic, W. J. Akers, L. Song, S. Achilefu, J. A. Margenthaler, M. D. Pashley, L. V. Wang *J. Biomed. Opt.* **2010**, *15*, 046010.

[17] L. V. Wang, J. Yao *Nat Methods*. **2016**, *13*, 627-638.

[18] A. Taruttis, V. Ntziachristos *Nat Photonics*. **2015**, *9*, 219-227.

[19] L. V. Wang, S. Hu *Science*. **2012**, *335*, 1458-1462.

[20] P. Beard *Interface Focus*. **2011**, *1*, 602-631.

[21] G. Diot, A. Dima, V. Ntziachristos *Opt. Lett.* **2015**, *40*, 1496-1499.

[22] P. K. Upputuri, M. Pramanik *J. Biomed. Opt.* **2017**, *22*, 041006.

[23] S. Hu *IEEE Journal of Selected Topics in Quantum Electronics*. **2016**, *22*, 6800610.

[24] C. Xie, P. K. Upputuri, X. Zhen, M. Pramanik, K. Pu *Biomaterials*. **2017**, *119*, 1-8.

[25] K. Sivasubramanian, M. Mathiyazhakan, C. Wiraja, P. K. Upputuri, C. Xu, M. Pramanik *J. Biomed. Opt.* **2017**, *22*, 041007.

[26] Y. Gawale, N. Adarsh, S. K. Kalva, J. Joseph, M. Pramanik, D. Ramaiah, N. Sekar *Chemistry - A European Journal*. **2017 (In Press)**, *23*.

[27] S. Huang, P. K. Upputuri, H. Liu, M. Pramanik, M. Wang *Journal of Materials Chemistry B.* **2016**, *4*, 1696-1703.

[28] C. Kim, C. Favazza, L. V. Wang *Chem. Rev.* **2010**, *110*, 2756-2782.

[29] G. P. Luke, A. Bashyam, K. A. Homan, S. Makhija, Y. S. Chen, S. Y. Emelianov *Nanotechnology*. **2013**, *24*, 455101.

[30] D. Pan, X. Cai, C. Yalaz, A. Senpan, K. Omanakuttan, S. A. Wickline, L. V. Wang, G. M. Lanza *Acs Nano*. **2012**, *6*, 1260-1267.

[31] D. Pan, M. Pramanik, A. Senpan, S. Ghosh, S. A. Wickline, L. V. Wang, G. M. Lanza *Biomaterials*. **2010**, *31*, 4088-4093.

[32] M. Pramanik, K. H. Song, M. Swierczewska, D. Green, B. Sitharaman, L. V. Wang *Phys. Med. Biol.* **2009**, *54*, 3291-3301.

[33] C. Kim, K. H. Song, F. Gao, L. V. Wang *Radiology*. **2010**, *255*, 442-450.

[34] K. H. Song, C. Kim, K. Maslov, L. V. Wang *Eur. J. Radiol.* **2009**, *70*, 227-231.

[35] J. Kim, S. Park, Y. Jung, S. Chang, J. Park, Y. Zhang, J. F. Lovell, C. Kim *Sci. Rep.* **2016**, *6*, 35137.

[36] K. H. Song, E. W. Stein, J. A. Margenthaler, L. V. Wang *J. Biomed. Opt.* **2008**, *13*, 054033.

[37] S. Prahl, M. Blue, W. To in Tabulated Molar Extinction Coefficient for Methylene Blue in Water, Vol. (Ed.^Eds.: Editor), City, pp.2-7.

[38] K. Sivasubramanian, V. Periyasamy, K. K. Wen, M. Pramanik *J. Biomed. Opt.* **2017**, *22*, 041008.

[39] in American National Standard for Safe Use of Lasers ANSI Z136.1-2000 (American National Standards Institute, Inc., New York, NY, 2000), Vol. (Ed.^Eds.: Editor), City.

[40] K. Sivasubramanian, M. Pramanik *Biomed. Opt. Express*. **2016**, *7*, 312-323.

[41] G. A. Chapman, D. Johnson, A. R. Bodenham *Anaesthesia*. **2006**, *61*, 148-158.

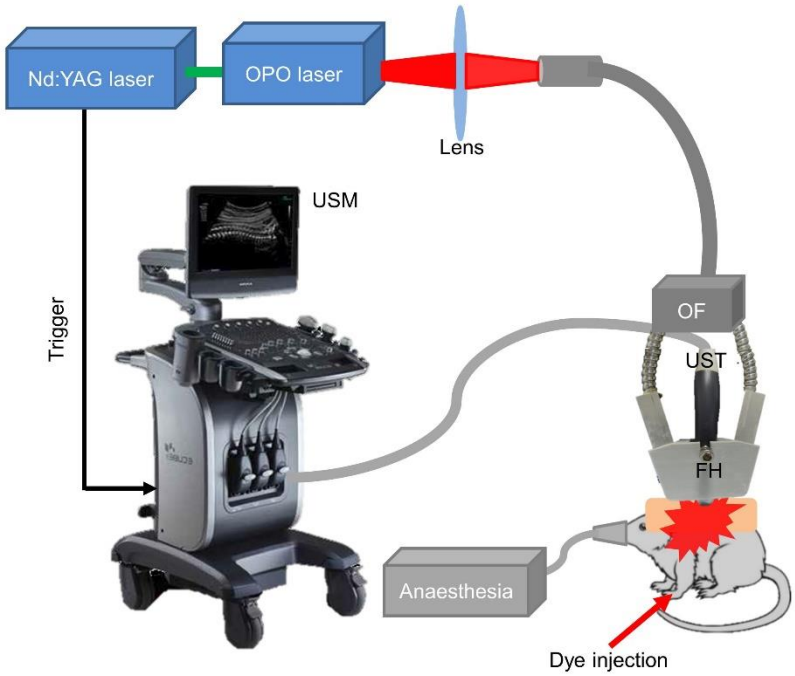

Figure 1. Schematic representation of the Photoacoustic imaging system with clinical ultrasound platform. OPO - optical parametric oscillator, OF - optical fiber bundle, FH – 3D printed fiber holder, USM - clinical ultrasound machine, UST- ultrasound transducer. The fiber holder houses the two output optical fiber bundle for illumination of tissue and ultrasound transducer for signal acquisition. An anaesthesia machine supplying isoflurane and oxygen was used to maintain the animal under anaesthesia for the duration of the experiments.

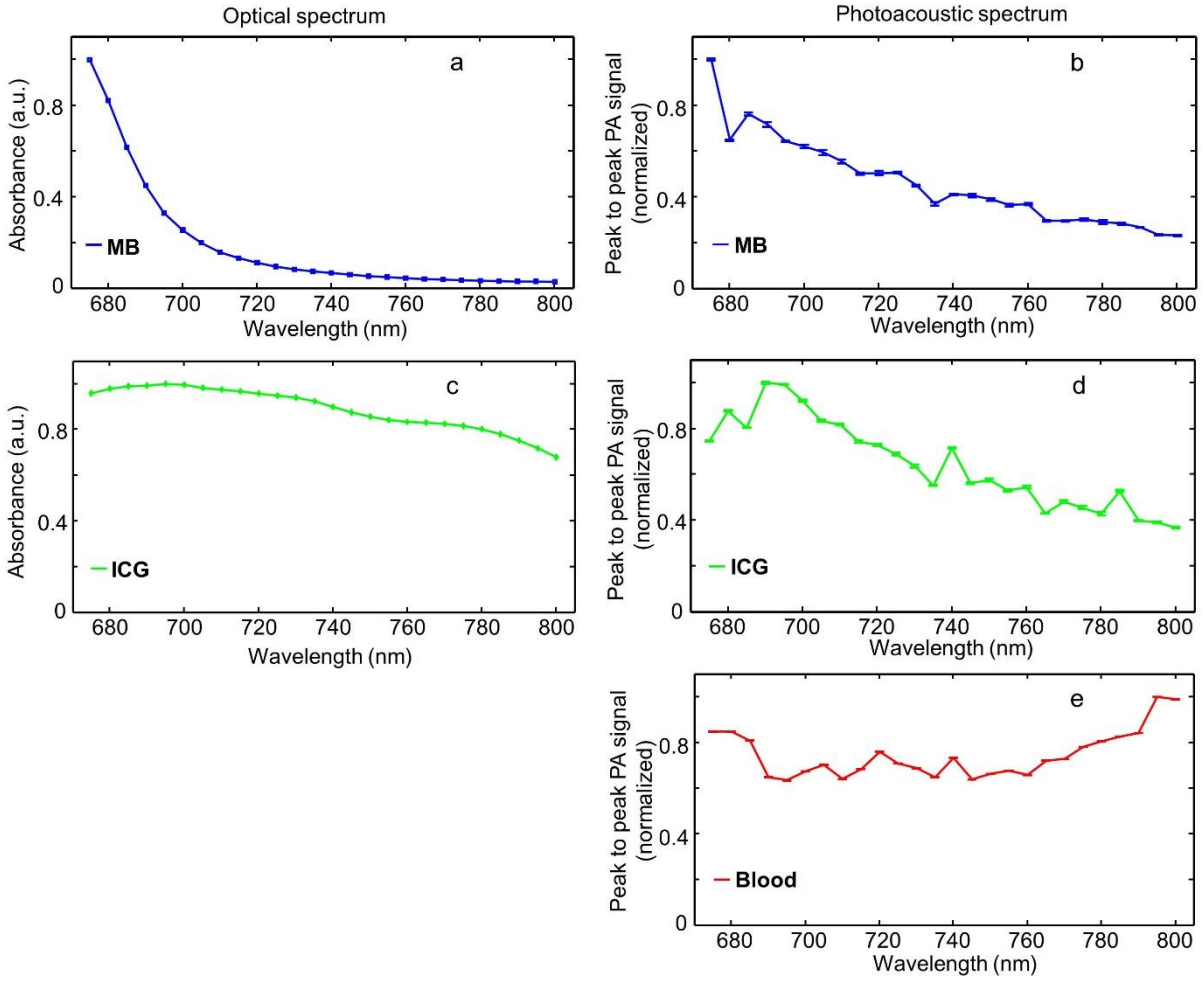

Figure 2. (a) Optical spectrum of methylene blue (MB) in the near infrared (NIR) range, (b) photoacoustic spectrum of the MB in the NIR wavelength range, (c) optical spectrum of indocyanine green (ICG) in the NIR range, (d) photoacoustic spectrum of the ICG in the NIR wavelength range, (e) photoacoustic spectrum of rat blood in the NIR wavelength range. The PA signals were normalized by the laser energy at each wavelength. 675 nm to 800 nm wavelength range with 5 nm step was used for both optical and photoacoustic spectra.

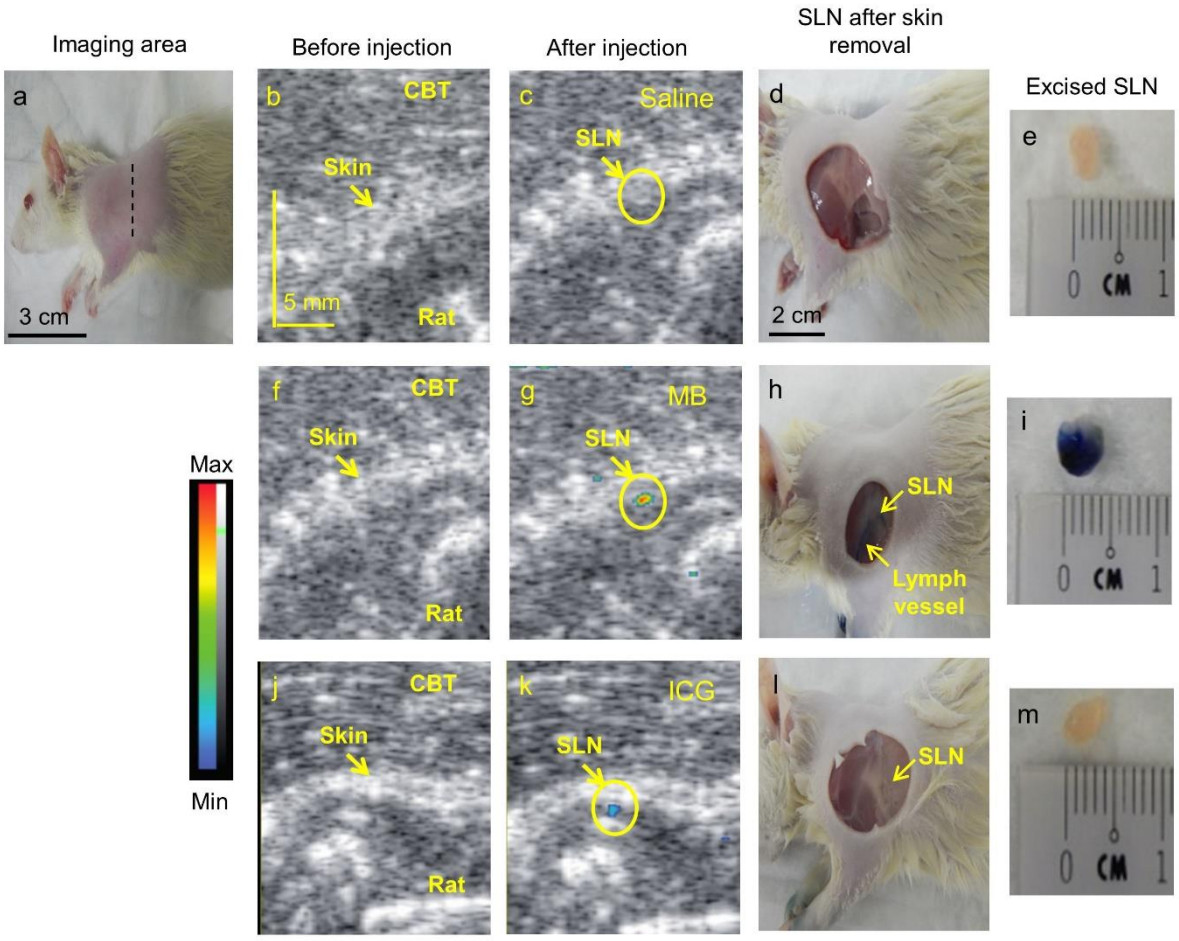

Figure 3. (a) Photograph of the shaved imaging region of the rat for SLN imaging, black dotted line shows roughly the plane across which B-scan ultrasound as well as photoacoustic imaging were done, (b) combined US and PA image before saline injection, (c) combined US and PA image after saline injection, (d) photograph of SLN after skin removal, (e) photograph of excised SLN, (f) combined US and PA image before MB injection, (g) combined US and PA image after MB injection, (h) photograph of SLN after skin removal, (i) photograph of excised SLN, (j) combined US and PA image before ICG injection, (k) combined US and PA image after ICG injection, (l) photograph of SLN after skin removal, (m) photograph of excised SLN. 675 nm wavelength was used for PA imaging with saline and MB, 690 nm wavelength was used for imaging with ICG. CBT - chicken breast tissue.

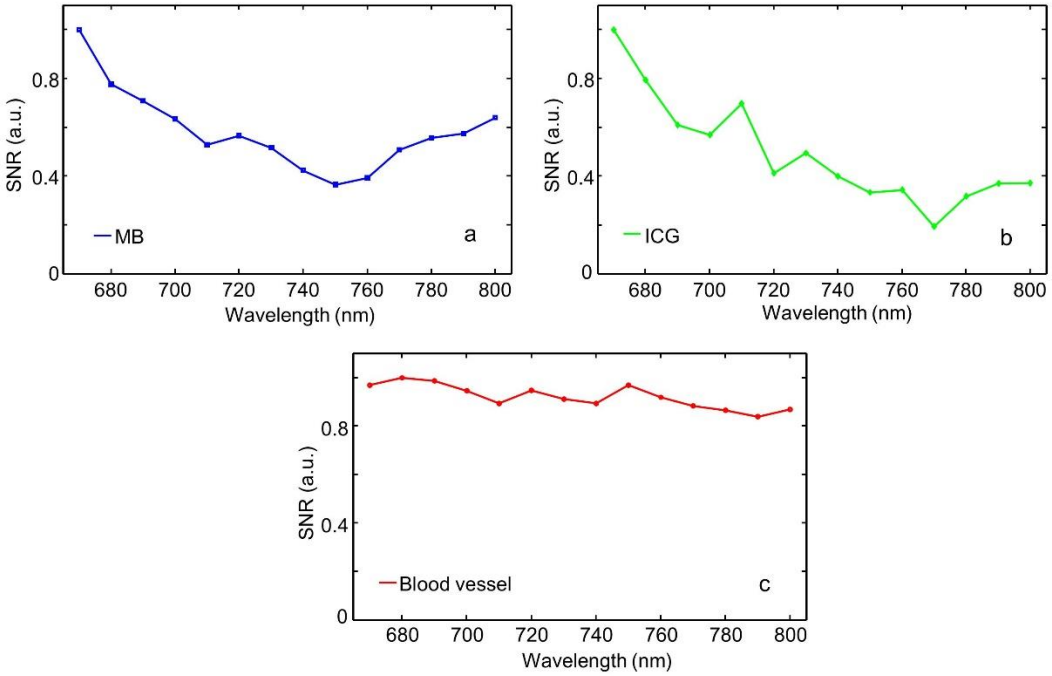

Figure 4. (a) PA spectrum obtained from the *in vivo* PA images (in terms of SNR) of the rat SLN with methylene blue, (b) PA spectrum obtained from the *in vivo* PA images of the rat SLN with indocyanine green, (c) PA spectrum obtained from *in vivo* PA images of the rat blood vessel. SNR was calculated for different wavelengths and normalised with the power of the laser. Movie S1 and movie S2 shows the combined PA and ultrasound imaging as the laser wavelength was scanned from 670 to 800 nm (for MB and ICG, respectively).

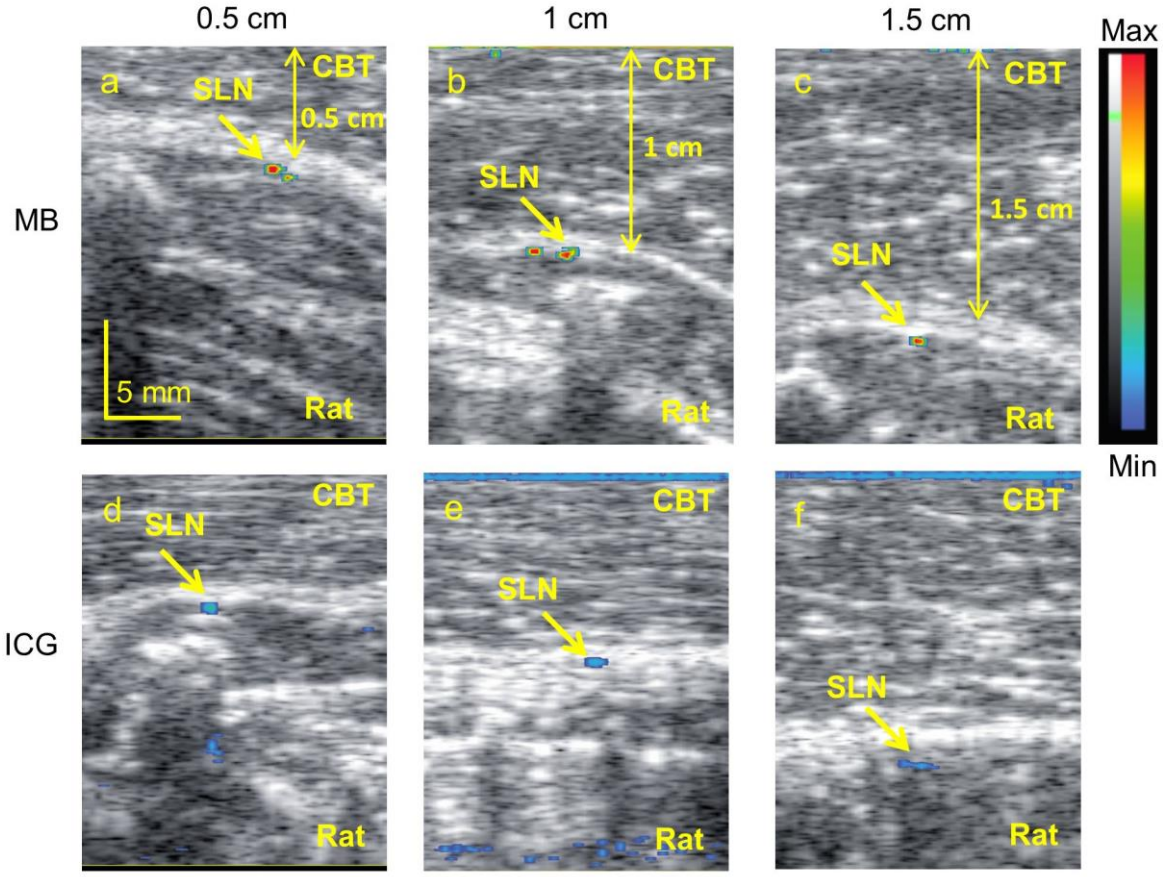

Figure 5. Combined PA and US images of (a) SLN filled with MB at 0.5 cm depth, (b) SLN filled with MB at 1 cm depth, (c) SLN filled with MB at 1.5 cm depth, (d) SLN filled with ICG at 0.5 cm depth, (e) SLN filled with ICG at 1 cm depth, and (f) SLN filled with ICG at 1.5 cm depth. CBT- Chicken breast tissue. The imaging depth were varied by stacking layers of CBT on top of the rat.

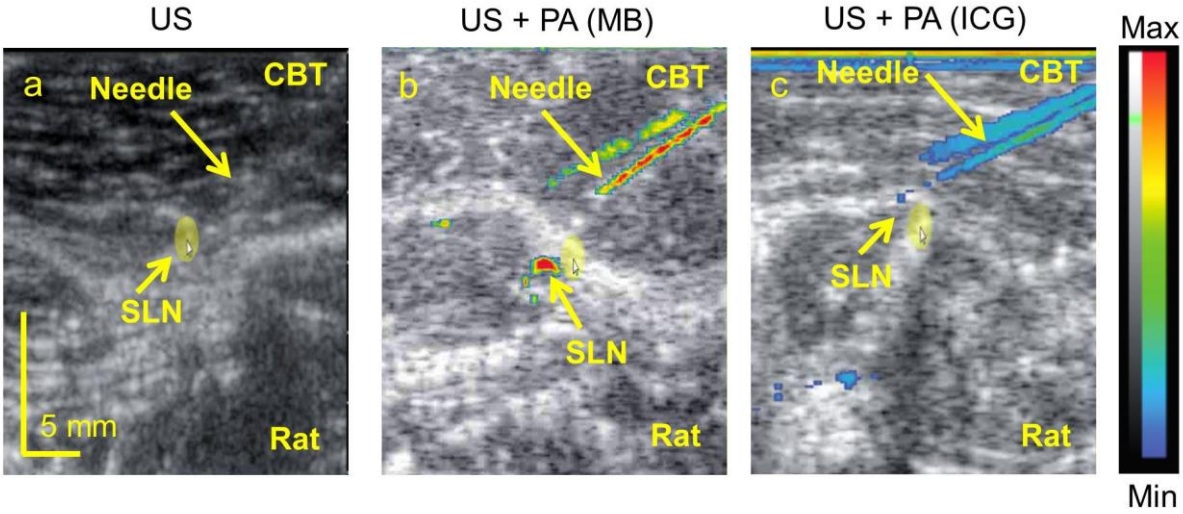

Figure 6. (a) US image showing the needle tracking as indicated by the yellow arrow, (b) combined US and PA image showing the needle reaching the sentinel lymph node filled with methylene blue, (c) combined US and PA image the needle reaching the sentinel lymph node filled with indocyanine green. CBT- Chicken breast tissue. Movie S3, movie S4, and movie S5 show non-invasive, real time needle tracking and guidance with US imaging only, under photoacoustic imaging (SLN filled with MB), and under photoacoustic imaging (SLN filed with ICG), respectively.

Graphical Abstract

Invasive breast cancer is one of the leading causes of cancer deaths in women. Identifying metastasis is very critical for prognosis of patient. Non-invasive imaging for diagnosing and staging breast cancer metastasis is much needed to overcome the complications associated with surgery. In this work, a clinical dual modal photoacoustic and ultrasound imaging system is used for non-invasive imaging of sentinel lymph nodes using methylene blue and indocyanine green as contrast agents. Non-invasive real time needle guidance to perform fine needle aspiration biopsy is also demonstrated.